The Viscoelastic Characterisation of Asphalt Mixtures Using the Indentation Test

Hassan Fadil[a], Feng Chen[a,*], Denis Jelagin[a], Manfred N. Partl[a,b]

[a] *Department of Civil and Architectural Engineering, KTH – Royal Institute of Technology Stockholm, Sweden*

[b] *Road Engineering/Sealing Components Laboratory, Empa - Swiss Federal Laboratories for Materials Science and Technology, Switzerland*

* Corresponding author:

Feng Chen

+46 76 715 56 99

feng.chen@abe.kth.se

"This is an Accepted Manuscript of an article published by Taylor & Francis in Road Materials and Pavement Design on 13th April 2021, available online: https://www.tandfonline.com/doi/10.1080/14680629.2021.1907218"

The Viscoelastic Characterisation of Asphalt Mixtures Using the Indentation Test

Viscoelastic characterization of asphalt mixtures is an important component for modelling and performance prediction of flexible pavements. In this study, a potential use of spherical indentation testing for the measurement of asphalt's viscoelastic properties is explored. Indentation testing may provide an interesting alternative to existing experimental techniques, as it allows for characterization of small material volumes. It may thus become a useful tool for the characterisation of thin asphalt layers, as well for measurement of binder phase properties *in situ* in asphalt mixtures. In the present study, spherical indentation tests are performed on two mastic asphalt (MA) mixtures, prepared with different mastic types. The shear relaxation moduli obtained from the indentation tests are compared with the ones measured with seismic and SuperPave Indirect Tensile (IDT) tests. A new statistical analysis methodology is proposed for viscoelastic characterization of the mastic phase with the indentation tests performed on MA mixtures. The accuracy and the sensitivity of the developed method is examined.

Keywords: indentation; asphalt mixtures; bitumen-filler mastic; multiscale; viscoelasticity.

1. Introduction

Field performance of asphalt mixtures is highly dependent on their viscoelastic properties (Elseifi, Al-Qadi, & Yoo, 2006). Accurate measurement of viscoelastic properties of asphalt mixtures as well as of their evolution during service life is thus a problem of significant practical importance, related to the construction quality control, pavement performance prediction and long-term performance monitoring. This study aims to contribute to this important topic by proposing a new spherical indentation test to characterise the viscoelastic properties of asphalt mixtures. Viscoelastic characterisation of asphalt mixtures with indentation testing is potentially advantageous as compared to other experimental techniques. Namely, the testing procedure is relatively simple and, except for the flat surface, the test does not have any requirements on specimen geometry. Furthermore, highly localised stress field induced during the test allows for measurements to be performed on small volumes in a relatively straightforward manner. It may thus become a useful tool for viscoelastic characterisation of thin asphalt layers, such as

surface courses, as well for monitoring of viscoelastic properties of binder phase *in situ* in asphalt mixtures.

In several recent studies, various versions of indentation tests have been applied for the characterisation of bitumen and bitumen-based materials, such as bituminous mastic and asphalt mortar. A number of studies have shown the potential of indentation tests for measuring viscoelastic properties of bitumen, by either using a flat or spherical indenters (Jelagin & Larsson, 2013; Zofka & Nener-Plante, 2011). Spherical indentation has also been applied for viscoplastic characterisation of bitumen and asphalt mixtures at large deformation (Ossa & Collop, 2007; Ossa, Deshpande, & Cebon, 2005).

In a recent study by Fadil, Jelagin, and Larsson, (2018) a new methodology for viscoelastic characterisation of bituminous material with spherical indentation test has been proposed, which allows extracting the linear viscoelastic properties at arbitrary non-decreasing loading. The technique proposed by Fadil et al. has also been extended to viscoelastic characterisation of binder-aggregate composites, such as fine sand asphalt mortar, by Fadil, Jelagin, Larsson, and Partl, (2019). Based on the modelling and experimental findings, it was shown in their study that the measurement scale in indentation tests is effectively controlled by the size of the indenter-specimen contact area. Performing indentation testing at different contact area sizes allows thus for reliable characterisation of materials relaxation modulus on both the macro-scale as well as on the scale of mastic phase. The present study aims to extend the methodology proposed by Fadil et al. for the characterisation of coarse binder-aggregate composites, such as asphalt mixtures. The asphalt's viscoelasticity is mainly controlled by the mastic phase, and, in fact, in several recent studies mastic's properties have been successfully related to mixtures performance with respect to cracking and rutting (Büchner & Wistuba, 2020). In this study, the particular attention is thus also given to identification of viscoelastic properties of mastic phase from indentation tests performed on asphalt mixture.

Spherical indentation tests are performed on two mastic asphalt (MA) mixtures, prepared with different mastic types, but with identical volumetric compositions. Methodology developed by Fadil et al. (2018) is employed to obtain shear relaxation modulus from the tests measurements. Mastic asphalt is chosen for this study as relatively simple type of asphalt mixture, due to the absence of air voids and relatively high mastic content. The shear relaxation moduli obtained from the indentation tests are compared with the mixture's viscoelastic properties measured with seismic and SuperPave Indirect

Tensile (IDT) tests. In order to identify the mastic phase properties from the indentation tests performed on MA mixtures, a statistical analysis methodology is proposed based on the Gaussian mixture model. This statistical analysis methodology has been utilised for indentation tests on composite materials by other researchers (Constantinides, Ravi Chandran, Ulm, & Van Vliet, 2006; Ulm et al., 2007). The accuracy and the sensitivity of the developed method is examined, based on a comparison with the Dynamic Shear Rheometer (DSR) measurements on mastics.

2. Problem Formulation and Methodology

This study is focused on the evaluation of the indentation test potential to be used for viscoelastic characterisation of asphalt mixtures. In this section, spherical indentation test procedure is briefly described and a methodology for determining a shear relaxation function, $G(t)$, from the test measurements is summarised. Asphalt mixtures are heterogeneous materials, containing generally three different phases: viscoelastic binder, elastic aggregates and air voids. Mastic asphalt (MA), a material of interest for this study, has, however very low air-voids content, thus, it may be considered as a two-phase composite. In this context, indentation testing has a unique potential as it allows the characterisation of the viscoelastic properties of binder-aggregate composites on both the macro- as well as on mastic scale, as shown by Fadil et al. (2019) for the case of asphalt mortar characterisation. Presently, a methodology proposed in their study is extended with an analysis procedure, based on the Gaussian mixture model, which is a technique used to identify different phases from the indentation test measurements on heterogeneous materials (Constantinides et al., 2006; Ulm et al., 2007). This technique is suitable for characterisation of coarse binder-aggregate composites, such as mastic asphalt.

A basic sketch of the spherical indentation test setup is shown in Figure 1(a). During the test a relatively rigid spherical indenter is pressed into the flat specimen in a displacement controlled mode, while indentation depth, $h(t)$, and the contact load, $P(t)$ are continuously recoded during the whole testing period. Detailed sketch of indentation process, is shown in Figure 1(b) along with the notation and coordinate system used in this study. For an isotropic linear viscoelastic specimen, it's mechanical behaviour can be described using two independent relaxation functions: shear, $G(t)$ and volumetric, $K(t)$.

Alternatively, the volumetric viscoelastic behaviour can be characterised using viscoelastic Poisson's ratio, $\nu(t)$.

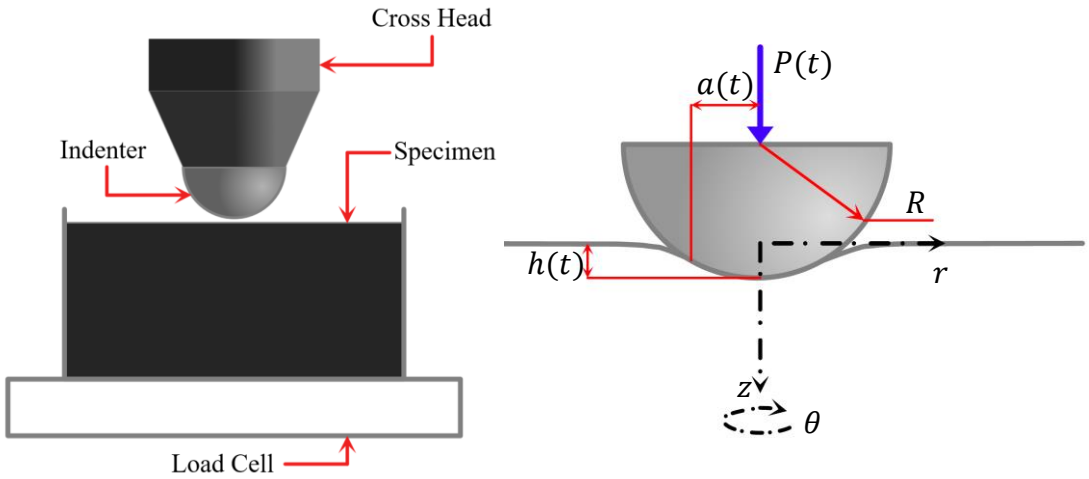

(a) (b)

Figure 1: (a) A Sketch of an indentation test setup, (b) a schematic showing the parameters used in the analysis method

A methodology for determining $G(t)$ from indentation tests performed at arbitrary non-decreasing loading has been developed by Fadil et al. (2018). As discussed in their study, the proposed analysis procedure allows overcoming the limitations associated with performing indentation tests following strict relaxation or creep loading histories. The solution is based on the Hertz solution for a frictionless indentation of a rigid spherical indenter into a linear elastic half-space, c.f. (Hertz, 1881; Johnson & Keer, 1986):

$$P = \frac{8}{3}\frac{G \cdot a^3}{(1-\nu)\cdot R}, \tag{1}$$

where P is the contact load, a is the contact area radius and R is the curvature of the spherical indenter.

The contact area radius is related to the indentation depth h as follows:

$$a = \sqrt{h \cdot R}. \tag{2}$$

The viscoelastic counter-part of Equation 1 may be obtained by utilising Lee's and Radok's method of functional integrals (Lee & Radok, 2011). For the particular case, of the constant viscoelastic Poisson's ratio i.e., $\nu(t) = \nu_o$, the relationship between the measured $h(t)$ and $P(t)$ is as follows:

$$P(t) = \frac{8}{3(1-\nu_o)}\sqrt{R}\int_0^t G(t-\tau)\times\frac{dh^{\frac{3}{2}}(\tau)}{d\tau}d\tau, \quad (3)$$

where R is the curvature radius of the indenter and τ is a dummy integration variable. Equation 3 is valid for arbitrary non-decreasing loading.

For bituminous materials, with profound relaxation properties, it is advantageous to use a two stage loading history, consisting of the loading stage where $h(t)$ is increased monotonically to the target indentation depth h_t, followed by the second stage where the indentation depth is kept constant. The actual indentation depth imposed on a specimen may furthermore be affected by machine compliance, C_m. Thus, the $h(t)$ imposed in the indentation test is defined through the following equation:

$$h(t) = \begin{cases} \frac{t}{t_r}h_t - P(t) * C_m & for\ t \le t_r \\ h_t - P(t) * C_m & for\ t \ge t_r \end{cases} \quad (4)$$

The shear relaxation modulus $G(t)$ is obtained from the $P(t)$ and $h(t)$ measured during the test by solving numerically the integral equation (3).

The length-scale of the indentation test measurements is controlled by the size of indenter-specimen contact area, as the measured response is dominated by the properties of the material in the vicinity of the contact area. As shown numerically and experimentally in Jelagin and Larsson (2013) and Fadil et al. (2019) for the cases of characterisation of binder-aggregate composites, the indentation test measurements are sensitive to the properties of the material within distance of approximately $5a$ from the indentation point. Accordingly, for the case of indentation tests on asphalt mixtures, a significant scatter in the measurements may be expected, as the materials local volumetrics (and thus its local viscoelastic properties) may vary significantly. This is further illustrated in Figure 2(a), where a sketch of indentation test on MA mixture, consisting of mastic (binder mixed with fines) and aggregates, is presented. The specimen's volume affected during the test is also marked in Figure 2(a). Depending on the point of indentation the measured response will either be dominated by the aggregates or by the mastic phase. A typical distribution of relaxation moduli from the indentation tests on mastic asphalt is illustrated in Figure 2(b), which shows a typical distribution of $G(t)$ taken at a fixed time $t = const$. In this Figure 2(b), the $G(t = const)$ data is shown

divided into two clusters representing the mastic dominated and aggregate dominated measurements.

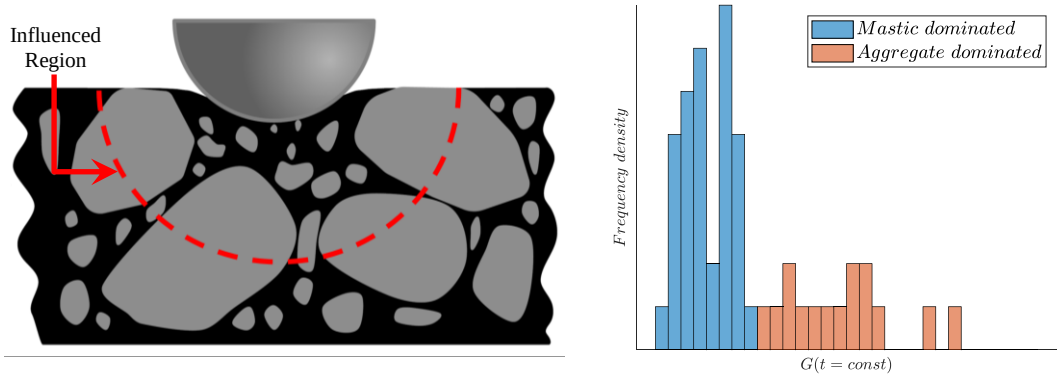

(a) (b)

Figure 2: (a) A sketch of indentation on binder-aggregate composites, (b) the clustering of data at certain point in time, $G(t = const)$

In order to separate the data into different clusters representing the phases in the material, the Gaussian mixture model (Constantinides et al., 2006; Ulm et al., 2007) was used. This is a probabilistic model allowing to identify the presence of subpopulations, representing the phases, within the measurements. In this study, mastic- and aggregate dominated measurements are assumed to have their own normal distribution with a mean value μ_i and standard deviation σ_i, where i is the subpopulation/phase i.e. $i = 1, 2$.

$$PDF_i(x) = \frac{1}{\sigma_i\sqrt{2\pi}} e^{-\frac{1}{2}\left(\frac{x-\mu_i}{\sigma_i}\right)^2} \tag{5}$$

where PDF_i is the probability density function of the phase i and x is a data point, i.e. $x = G(t = const)$. These probability density functions of the separate phases are then combined together to form the probability density function for all measurements:

$$PDF_c(x) = f \cdot PDF_1(x) + (1 - f) \cdot PDF_2(x) \tag{6}$$

where PDF_c is the combined probability density function and f is the proportion contribution of phase $i = 1$.

For a given family of measurements, $G(t = const)$, parameters μ_i and σ_i may be identified using the iterative Expectation-Maximisation (EM) algorithm, implemented in MATLAB (Dempster, Laird, & Rubin, 1976).

Afterwards, the Gaussian mixture model is used to cluster the data, this is achieved by utilising Bayes rule and, specifically, calculating the membership score

which is the posterior probability Pr as calculated in Equation 7 and Equation 8 for each phase. Hard clustering is performed by assigning each data point to either mastic-dominated or aggregate dominated cluster.

$$Pr_1(x) = \frac{f \cdot PDF_1(x)}{PDF_c(x)} \tag{7}$$

$$Pr_2(x) = \frac{(1-f) \cdot PDF_2(x)}{PDF_c(x)} \tag{8}$$

The data point x is then determined to be part of the cluster that has the highest Pr_i value.

The methodology adopted in this paper is summarised in Figure 3. In order to account for the $G(t)$ measured over the whole range of the tests, the multivariate Gaussian mixture model was used, with clustering done based on $G(t)$ values measured at both the beginning and the end of indentation test.

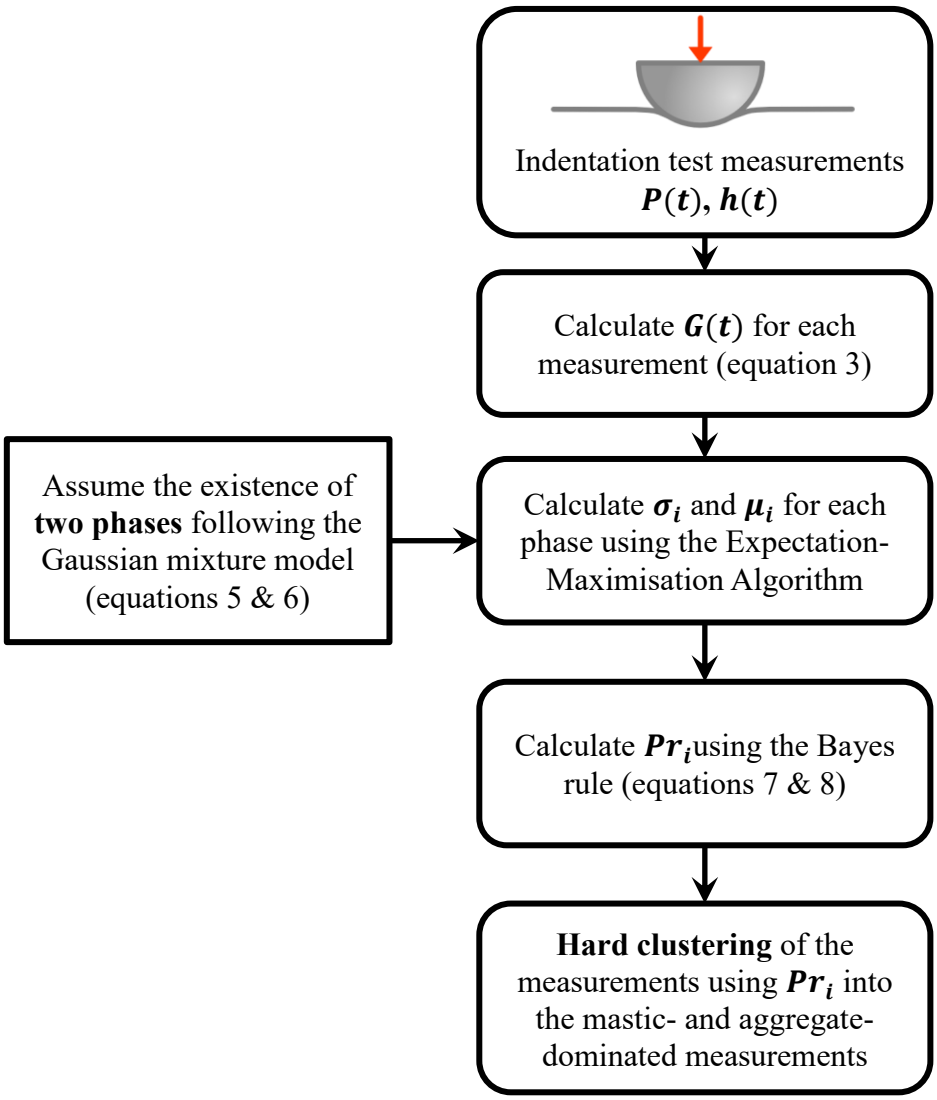

Figure 3: A schematic summarising the methodology adopted in this research

3. Experimental Study

Spherical indentation tests described above were applied to measure the relaxation modulus, $G(t)$, MA mixtures. In order to evaluate the sensitivity of the indentation tests to the mastic phase properties, two MA mixtures were manufactured having identical volumetric composition and different mastics. $G(t)$ measured from indentation tests were compared with the Indirect Tensile (IDT) creep tests and seismic tests, as well as rheological properties of the mastics measured with the Dynamic Shear Rheometer (DSR).

3.1 Materials and Characterisation

3.1.1 Bitumen-filler mastic

Bitumen-filler mastic specimens were prepared in the laboratory, and a dynamic shear rheometer (DSR) was used to characterise their viscoelastic properties according to EN-14770. Two types of bitumen-filler mastic were made, by mixing neat bitumen 70/100 (Nynas AB, 2010) with 30% volume fraction of the two different fillers: (i) 30% hydrated lime filler (BL30) and (ii) quartz sand filler (BQ30), respectively. The densities of the two fillers were measured using the pycnometer method according to ISO 1183-1:2012, to be 2.378 ± 0.055 g/cm^3 and 2.687 ± 0.021 g/cm^3 for the hydrated lime and the quartz sand fillers respectively. DSR frequency-sweep tests, in the frequency range from 0.1 to 10 Hz, were performed on mastic specimens at temperatures of 0°C, 5°C and 10°C. Two replicates of each mastic were tested with a difference less than 20% between the results of $G^*(\omega)$. The results were shifted to the reference temperature $T_{ref} = 0$°C, where the master curve was constructed while assuming that the shift factors follow the Williams–Landel–Ferry equation. Figure 4 shows the DSR results of the complex modulus $G^*(\omega)$ and the phase angle $\delta^*(\omega)$ for the tested bitumen-filler mastics. From the comparisons, one can find BL30 mastic is significantly stiffer as compared to BQ30 mastic.

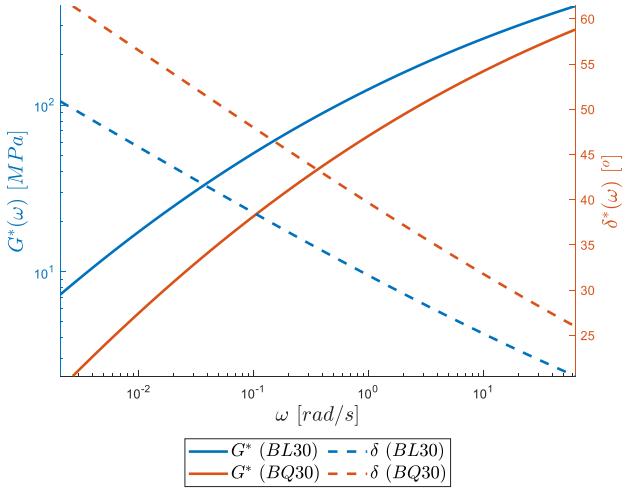

Figure 4: Complex modulus $G^*(\omega)$ and phase angle $\delta^*(\omega)$ results of two bitumen-filler mastics at $T_{ref} = 0$°C.

3.1.2 Mastic Asphalt mixture

Two MA mixtures having identical aggregate gradations but different mastics were manufactured. Specifically, the gradation of the MA is shown in Table 1, in which the content of fillers (i.e. fines smaller than 0.063 mm) is 22.5% by mass. Bitumen 70/100 was used as binder material in MA and the content is 8% by weight. The goal was to have mastic phase properties in MA mixtures as close as possible to the mastic specimens tested with DSR, accordingly the same filler and bitumen types as well as same volumetric filler contents of 30% were used. Cylindrical MA specimens, with filler types of Hydrated Lime (HL) and Quartz (QZ) sand, were prepared, with two replicates created for each MA type. The specimens had a diameter of 15.18 ± 0.19 cm and a thickness of 3.65 ± 0.35 cm. These specimens were used for the indentation, IDT as well as the seismic tests.

Table 1. Aggregate gradation of the MA mixture

Sieve size, mm	0.063	0.125	0.25	0.5	1	2	4	8	11.2	16	22.4	31.5
Pass, % by mass	22.5	26	30	36	42	47.5	56.5	68.5	78.5	92	100	100

Complex moduli $G^*(\omega)$ of MA mixture specimens were determined with a non-destructive seismic tests. The tests were performed by exciting the specimens using an impact hammer and measuring the resulting vibration of the specimens with an

accelerometer. Since the acoustic resonance frequencies of a solid are functions of the stiffness, mass, dimensions and boundary conditions under vibration, the complex modulus $G^*(\omega)$ can be derived from these measurements using suitable Frequency Response Functions (FRFs). A complete description of the measurement method can be found in Gudmarsson et al. (2014). In present study, seismic tests were carried out on the same MA specimens at three temperatures -20˚C, 0˚C and 15˚C. The seismic test results are shown in Figure 5(a). Due to the high binder contents in the mixtures the amount of damping was large and the results were limited to high frequencies i.e. $2 \cdot 10^4 - 18 \cdot 10^4$ rad/s, as seen in Figure 5(a). In the tested frequency range, the differences between the two tested materials are small (< 5 %). Moreover, there is no consistent ranking of the materials. The mixtures Poisson's ratio was found to be in the range from 0.29 to 0.38 from the seismic testing measurements.

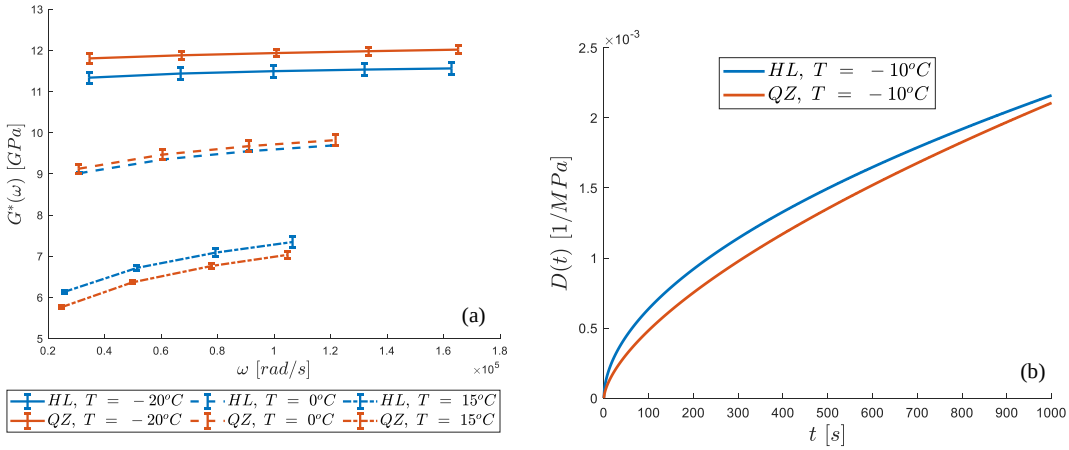

Figure 5: The properties of the HL and QZ samples as measured using the (a) seismic test and (b) Indirect tensile test (IDT)

IDT creep tests were further performed, following the procedure developed by Buttlar and Roque (1994), on the same MA mixtures to determine their viscoelastic response at longer relaxation times. A constant load was applied for 1000 s resulting in horizontal strain within the range of around 200-750 micro-strains, to ensure the deformations are close to the linear viscoelastic range. The tests were performed at a relatively low temperature of -10˚C, to minimise measurement errors due to gage drifting and non-viscoelastic deformations in specimens. The creep compliance from the test can be determined by:

$$D(t) = \frac{\Delta H \cdot th \cdot D \cdot C_{comp}(t)}{P \cdot GL}, \tag{9}$$

where, $D(t)$ is the creep compliance at time t; $C_{comp}(t)$ is the correction factor at time t; P is the maximum load; GL is the gauge length; ΔH is the horizontal deformation; th is the specimen thickness; D is the diameter of the specimen. The results of the Indirect tensile test (IDT) are shown in Figure 5(b), from which one can observe the creep compliance $D(t)$ of the MA mixture with hydrated lime (HL) mastic material to be somewhat higher than the one for the QZ material. For comparison with indentation test measurements, the relaxation modulus $G(t)$ of material was obtained from the creep compliance $D(t)$ using the viscoelastic correspondence principle:

$$G(t) = \mathcal{L}^{-1}\left\{\frac{1}{s^2 \cdot \widetilde{D}(s)}\right\}, \tag{10}$$

where,

$$\widetilde{D}(s) = \mathcal{L}\{D(t)\}. \tag{11}$$

Afterwards, the results were shifted to 0°C, using the shift factors obtained for the BL30 and BQ30 mastic materials as 0.0152 and 0.0162 respectively from the DSR measurements performed in a study by Fadil, Jelagin, and Partl (2020). Thus, the MA mixture with HL material is stiffer than the MA mixture with QZ material, in qualitative agreement with the DSR results in Figure 4.

3.2 Indentation Tests

Instrumented indentation tests were applied to measure the relaxation modulus $G(t)$ of the mastic asphalt (MA) mixtures. As shown in Figure 6, an MTS 810 hydraulic load frame and a steel spherical indenter with $R = 15.875$ mm were used in the customised test setup. A ramp-relaxation loading procedure, defined by Equation 4 was followed. Specifically, a displacement-controlled load was applied to indenter, reaching a fixed indention depth of 0.3 mm within 1 second. The $h_{max} = 0.3$ mm results, according to Equation 2 in maximum contact area radius of $a_{max} = 2.18$ mm. The load was then held constant for 100 s, and the reaction force $P(t)$ was continuously recorded. Based on the measured $P(t)$, the shear modulus $G(t)$ was calculated according to Equation 3, in which the machine compliance effects were also calibrated according to Equation 4. ν_o value in Equation 3 was taken to be 0.33, based on the average value obtained from the seismic tests.

Tests were carried out at two temperatures 0°C and 10°C, in which a 10 kN load cell was used at 0°C and a 1 kN load cell was used at 10°C, with the setup having a

measured machine compliance values C_m of $5.1 \cdot 10^{-5}$ and $15.6 \cdot 10^{-5}$ mm/N for each load cell respectively. For each MA material and at each temperature, indentation tests were applied at 50 randomly selected locations, guided by the sketched grid mesh that illustrated in Figure 6. The size of each mesh area was chosen to be 2×2 cm, in order to have the adjacent indentations at a distance of at least $10 \cdot a_{max}$ from each other.

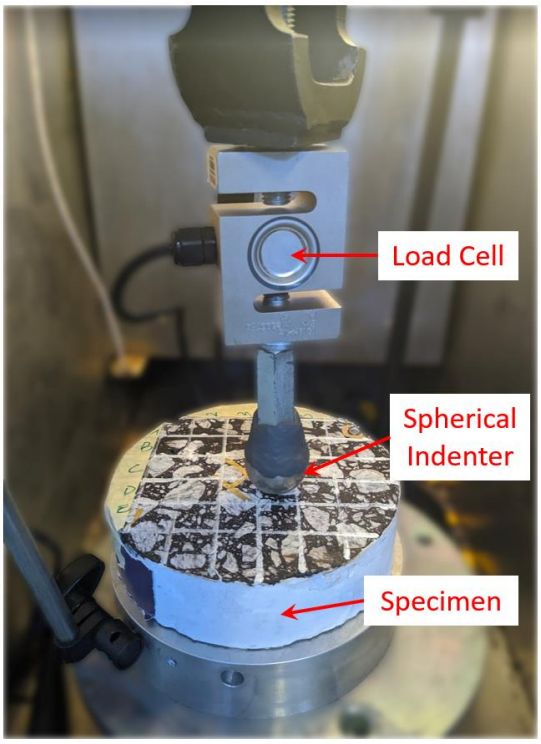

Figure 6: Instrumented indentation test on MA mixture

4. Results and Discussion

An example of $G(t)$ measured with indentation tests is presented in Figure 7(a) for the case of MA mixture with hydrated lime filler and $T = 0$˚C. The measurements obtained for the mixture with quartz filler and at $T = 10$˚C are qualitatively similar and are omitted here for briefness. In Figure 7(a), $G(t)$ obtained from the 50 indentation tests are presented.

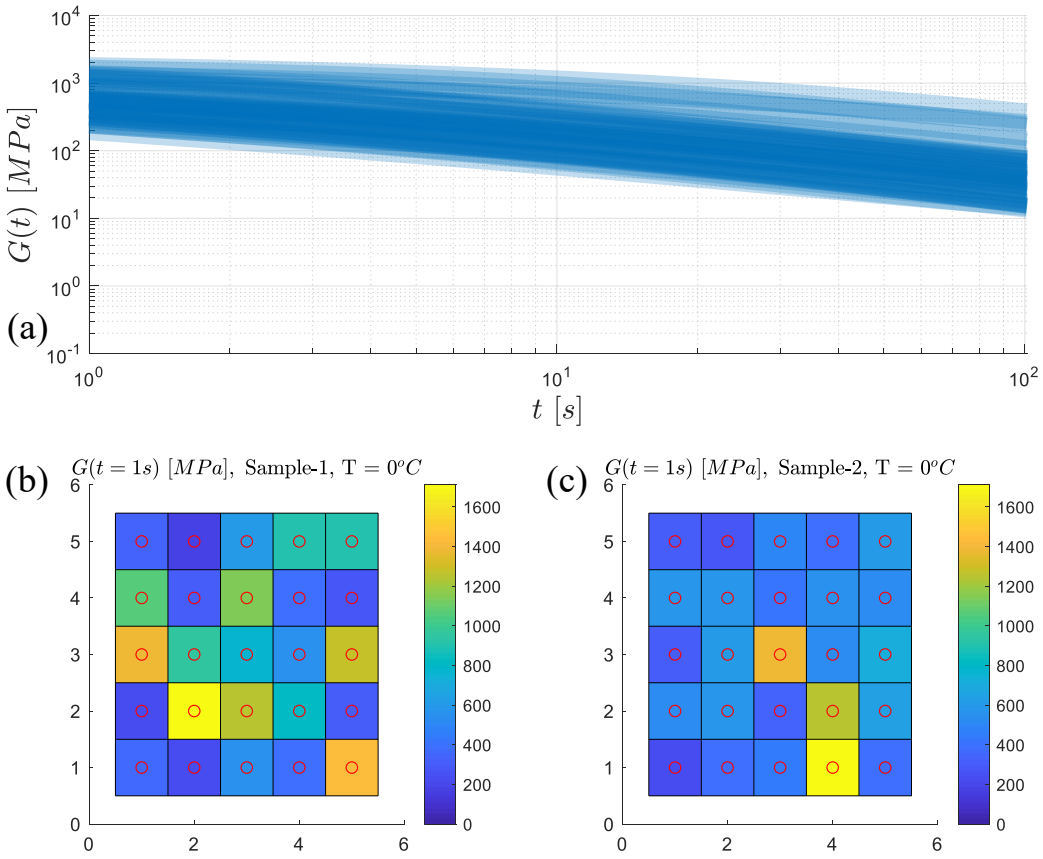

Figure 7: (a) $G(t)$ obtained from the indentation tests for the HL material at $T = 0$˚C, (b) $G(t = 1\ s)$ distribution on the surface of sample-1 and (c) on the surface of sample-2

As can be seen in Figure 7(a), $G(t)$ measured in all the tests decreases with time, following approximately a power-law function. At the same time, the measurements are accompanied by significant scatter, due to the inhomogeneity of the material. The scatter magnitude is furthermore dependent on the relaxation time, for example, for $t = 1\ s$ and $t = 100\ s$ $G(t)$ varies in the range between 180 - 3000 MPa and 10 - 400 MPa correspondingly. Spatial variation of the measurements is further illustrated in Figure 7(b,c) where the distribution of $G(t = 1s)$, measured at $T = 0$˚C, on the surface of the two HL replicates is shown. It can be seen that the variations presented in Figure 7(b,c) do not follow any obvious pattern and are thus caused by random variation of materials volumetric composition at the measurement point, as discussed in section 2 above.

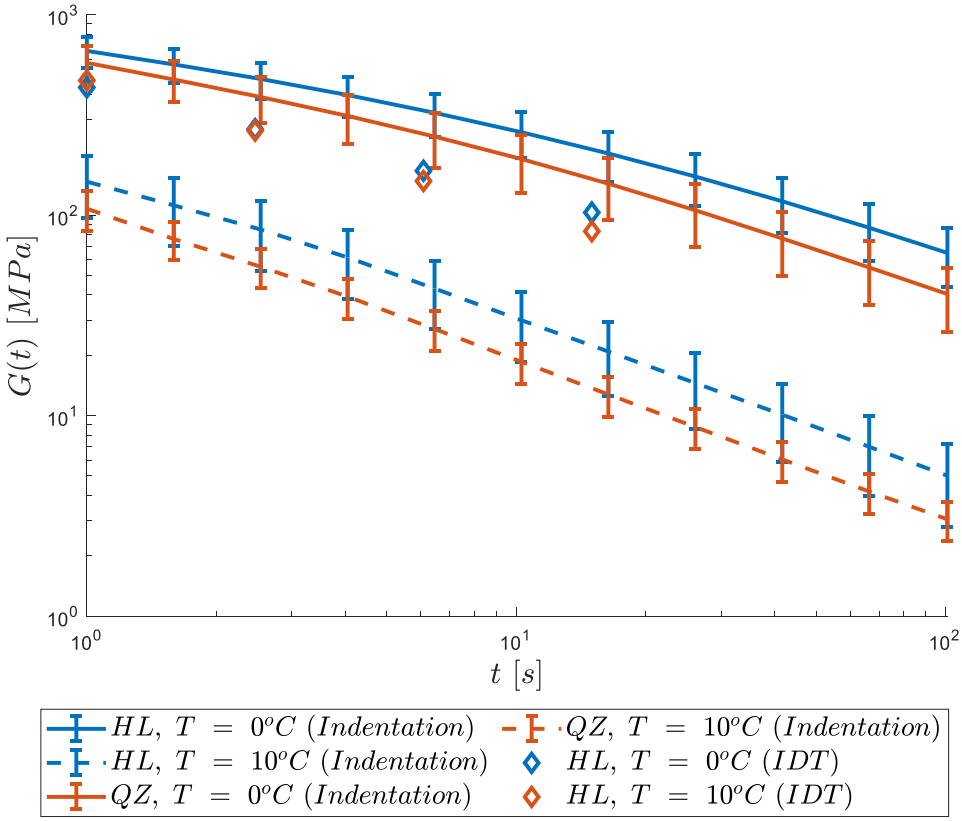

Figure 8: The mean $G(t)$ obtained from indentation tests for HL and QZ samples at $T =$ 0°C and 10°C, as well as form the IDT creep test at $T = 0$˚C, the error bars represent the 95% confidence interval.

The mean $G(t)$, obtained using indentation tests, is shown in Figure 8 along with 95% confidence intervals for both tested MA mixtures, HL and QZ, at the two test temperatures $T =$ 0°C and 10°C. Also in Figure 8, the $G(t)$ at $T =$ 0°C obtained for the two materials from the IDT creep test measurements are presented. As may be seen in Figure 8, the effect of temperature and of mastic properties on the indentation test measurements is qualitatively correct. As may be expected, based on the results presented in Figure 4, HL materials and lower temperatures result in higher mean relaxation moduli. It is worth noting however, that, for both temperatures examined, there is a significant an overlap in the indentation results for the QZ and HL materials, when the 95% confidence intervals are considered.

As also seen in Figure 8, at $T = 0$˚C the $G(t)$ obtained from the IDT creep test are at least within the same range with the indentation results, with the deviation between the two test methods being within 40% for the majority of the measurement interval. It has to be emphasised however, that exact quantitative agreement may not be expected,

due to different loading modes employed in the tests as well as due to the uncertainties related to the interconversion procedure employed to obtain $G(t)$ from IDT creep test measurements, cf. Equation 10. In summary, the results presented in Figure 8, indicate that the indentation test may be a viable alternative for viscoelastic characterisation of asphalt mixtures.

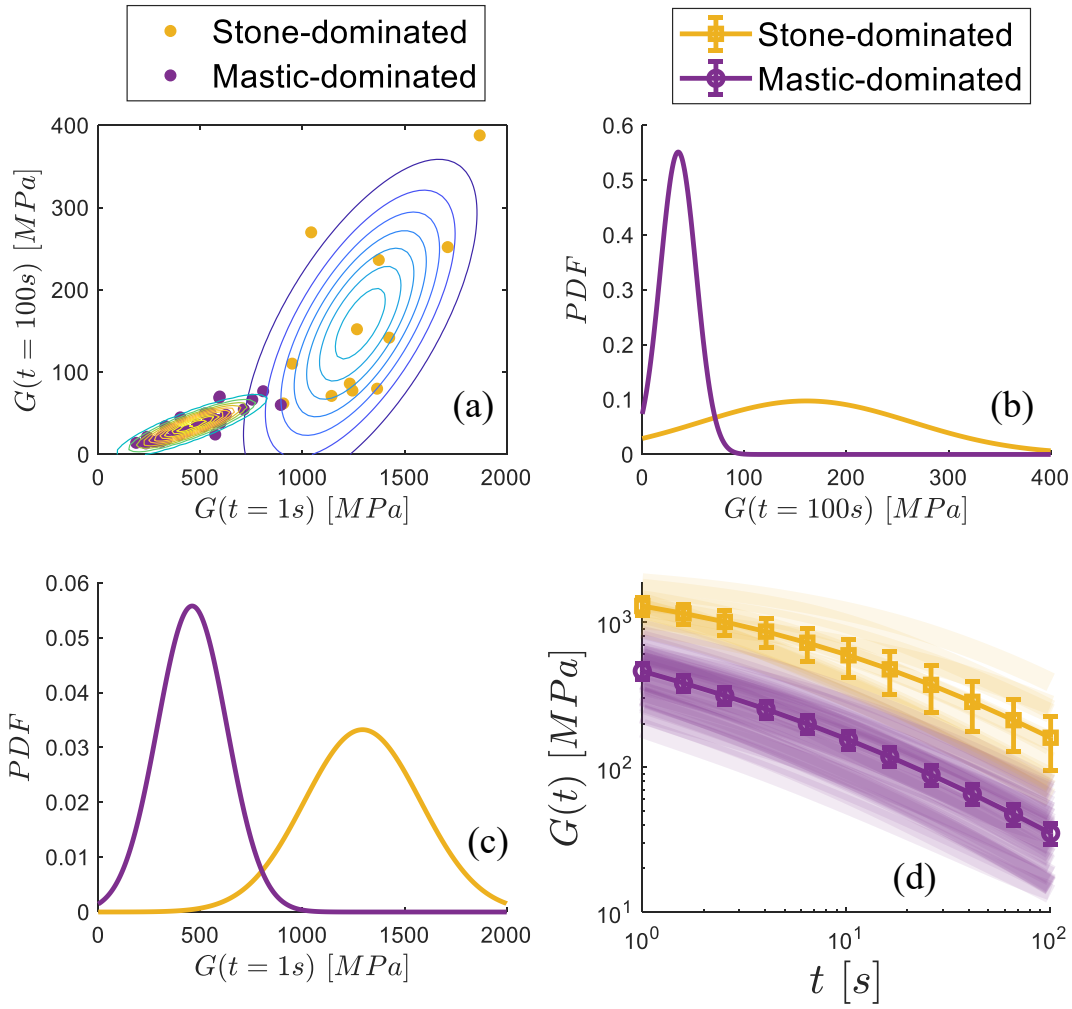

Figure 9: Clustering the measured data using the Gaussian mixture model for the HL samples at $T = 0$˚C: (a) contour plots of the probability density functions (PDF) for the two model parameters: $G(t)$ at $t = 1$s and 100 s; (b) normalised PDF of $G(t = 100\ s)$ and of (c) $G(t = 1\ s)$. (d) The result of phase separation: individual $G(t)$ measurements colour coded according to the phases.

In order to evaluate the possibility of using indentation testing for *in situ* measurement of mastic's viscoelastic properties, the $G(t)$ measured with indentation tests were divided into two clusters of mastics- and aggregate-dominated responses. The clustering has been performed, based on the $G(t)$ values measured at $t = 1\ s$ and 100s,

using the multivariate Gaussian model, described in the section 2. The $G(t)$ clustering process is illustrated in Figure 9 for the case of the tests performed on MA mixture with hydrated lime filler at $T = 0^{\circ}$C. In Figure 9(a) the $G(t)$ measured at $t = 1$ s to $t =$100 s are presented. It is clear from the figure that the data can be tentatively separated into two clusters: the measurements having a relatively low $G(t)$ values at both $t = 1$ s and $t =$ 100 s and the ones having higher $G(t)$ values at both *t*. This separation is performed by fitting normal probability distribution functions (Equation 5) into both clusters. The parameters μ_i, σ_i and f in Equations (5-6) are obtained with the iterative Expectation-Maximisation (EM) algorithm (Dempster et al., 1976) implemented in MATLAB. The contours of the PDFs obtained for the mastic- and aggregate-dominated measurements are also shown in Figure 9(a). The normalised PDFs for the two measurements clusters are further illustrated in Figure 9(b,c) for the cases of $G(t = 100\,s)$ and $G(t = 1\,s)$ respectively. As seen in Figure 9(b,c) the data corresponding to mastic dominated measurements has a significantly narrower distribution as compared to the aggregate dominated ones.

Once the parameters μ_i, σ_i and f are identified, the individual indentation test measurements can be attributed to either mastic- or aggregate-dominated responses through the use of Bayes rule and calculating the posterior probabilities (Equations 7 and 8). The outcome of the clustering procedure is shown in Figure 9(d), where the measured $G(t)$ values are shown and colour coded according to the cluster they are attributed to, together with the mean values of each cluster and their 95% confidence interval.

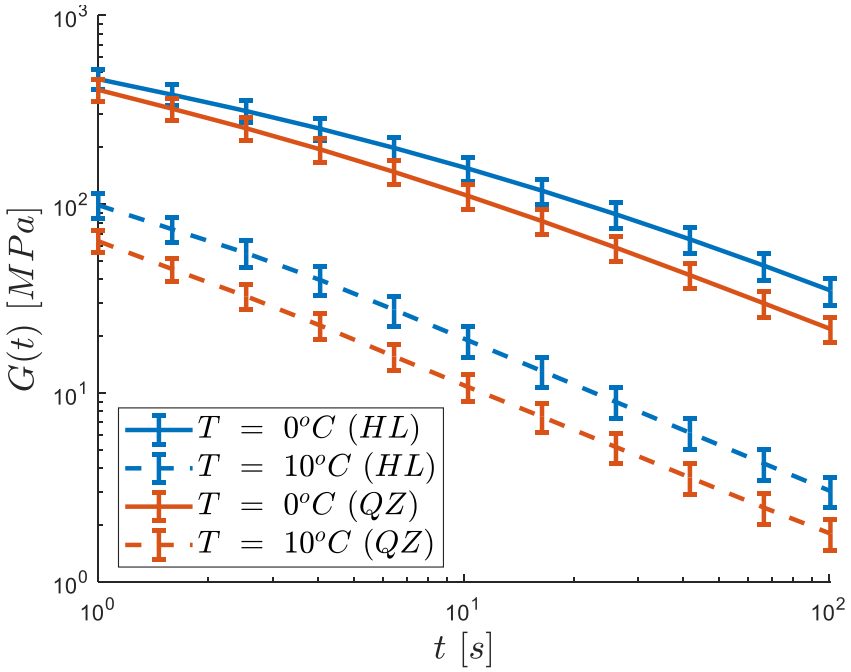

Figure 10: The mean $G(t)$ obtained from the mastic-dominated indentation tests; HL and QZ materials at $T = 0$°C and 10°C, the error bars represent the 95% confidence interval.

The mean $G(t)$ obtained from mastic-dominated indentation tests are presented in Figure 10 along with their 95% confidence intervals, for the HL and QZ materials and for $T = 0$°C and 10°C. As may be seen, the results presented in Figure 10, are approximately 1.5 to 2 times below the mean $G(t)$ for all the indentation tests presented in Figure 8. As observed in Figure 10, for both temperatures examined, $G(t)$ values for HL material are consistently higher as compared to the one for QZ material, which is in, at least, a qualitative agreement with the corresponding mastics properties measured with the DSR (Figure 4). Furthermore, the difference between the HL and QZ materials presented in Figure 10 is statistically significant, as may be seen by comparing their 95% confidence intervals. Thus, it may be concluded, that clustering based on the multivariate Gaussian mixture model, allows for successfully identifying mastic-dominated indentation test measurements.

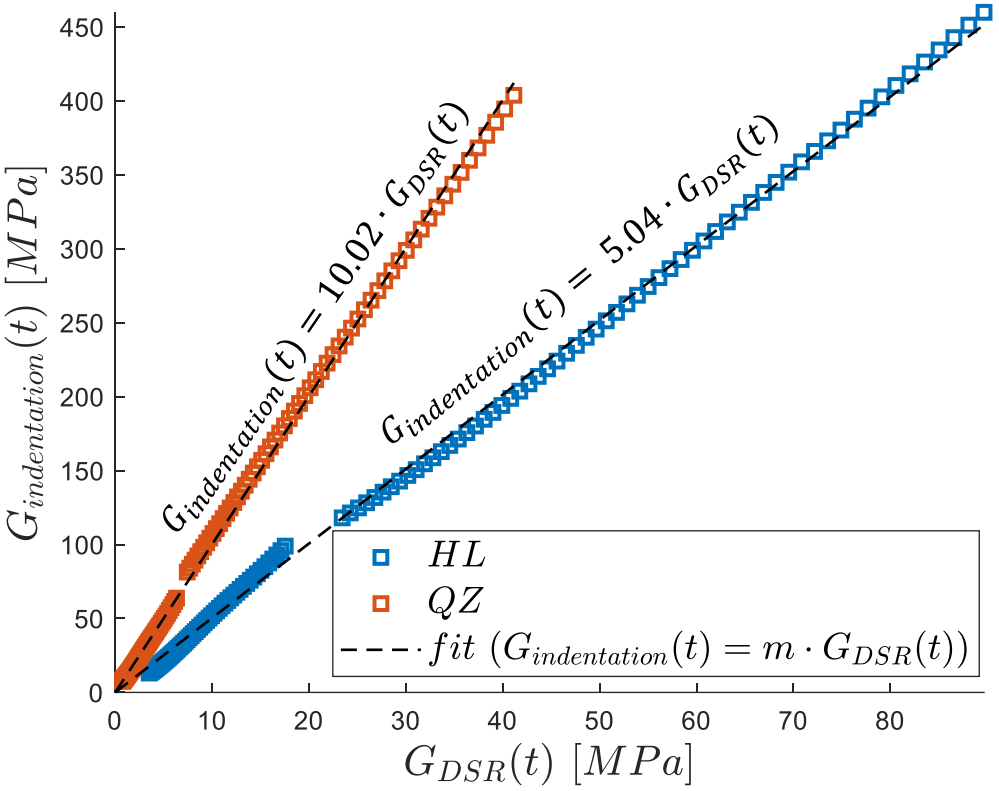

Figure 11: Correlation between the mean $G(t)$ obtained from the mastic-dominated indetation tests and the DSR results on corresponding mastic

The relationship between the indentation tests measurements and the viscoelastic properties of mastic phase is further explored in Figure 11, where $G(t)$ values obtained for HL and QZ materials with the mastic-dominated indentation tests are presented against $G(t)$ obtained with the DSR on the corresponding mastic materials. The results in Figure 11 are presented for both tested temperatures, i.e. $T = 0$°C and 10°C. As can be seen in the figure, $G(t)$ values from indentation tests are always significantly higher than the ones obtained from the DSR measurements. This is expected, given the scale of the indentation tests performed. In the present study, indentation tests where done at R and h combinations resulting in $a =$ 2.18 mm, according to Equation 2. This results in measurement volume size of approximately a sphere with a radius of 11 mm, meaning that all measurements are influenced by the presence of large aggregates to some degree. However, as seen in Figure 11, there exists a clear linear relationship between the indentation and DSR measurements:

$$G_{indentation}(t) = m \cdot G_{DSR}(t) \tag{12}$$

where m is the slope of the correlation line, which can be considered as multiplier that correlates the DSR measurements on mastics to the mastic-dominated indentation tests results. The value of m is 10.02 and 5.04 for QZ and HL correspondingly, indicating that this multiplier is dependent on the interaction between the mastic phase and the aggregates. As the results presented in Figure 10 and Figure 11 indicate, the indentation test combined Gaussian mixture model presents the possibility for gaining an insight into the viscoelastic properties of the mastic phase, from the *in situ* measurements performed on asphalt mixtures.

5. Conclusions

The feasibility of using spherical indentation tests for the viscoelastic characterization of asphalt mixtures and their mastic phases has been investigated. The tested mastic asphalt (MA) mixtures were prepared with the same binder type and volumetric composition, but two different filler types, resulting in difference in mastic's viscoelastic properties. Shear relaxation moduli, $G(t)$, of the two MA mixtures have been measured with the indentation tests, with 50 tests performed for each material and temperature. The measured $G(t)$ were found to have a large scatter, attributed to variations in materials volumetric composition near the indentation location. The mean $G(t)$ obtained from 50 tests were found to capture the effects of temperature and of mastic phase properties on the MA mixture well, as well as to be in a reasonable agreement with the results SuperPave IDT creep tests. The indentation testing may thus be potentially considered as a viable alternative to existing viscoelastic characterization methods, in particular as the test is non-destructive and can be used to characterise thin asphalt layers.

In order to gain better insight into mastic phase properties from the indentation tests performed on MA mixtures, a new statistical analysis procedure has been proposed. It is shown that the proposed procedure allows identifying clusters of measurements capturing the mastic- and aggregate-dominated responses of the asphalt mixture. The mean $G(t)$, obtained from the mastic-dominated indentation tests were found to be linearly related with the DSR measurements on the corresponding mastic, with a single multiplier correlating the indentation results to the DSR measurements on mastic. The obtained results indicate, that the developed testing technique allows for capturing mastic phase properties from measurements performed on MA mixtures without extracting the binder.

6. References

Büchner, J., & Wistuba, M. P. (2020). Relating Asphalt Mixture Performance to Asphalt Mastic Rheology. In *Proceedings of the 9th International Conference on Maintenance and Rehabilitation of Pavements—Mairepav9* (Vol. 76, pp. 639–649). https://doi.org/10.1007/978-3-030-48679-2_60

Buttlar, W., & Roque, R. (1994). Development and evaluation of the strategic highway research program measurement and analysis system for indirect tensile testing at low temperatures. *Transportation Research Record: Journal of the Transportation Research Board*, *1454*, 163–171. https://doi.org/10.1016/j.ijporl.2017.05.027

Constantinides, G., Ravi Chandran, K. S., Ulm, F. J., & Van Vliet, K. J. (2006). Grid indentation analysis of composite microstructure and mechanics: Principles and validation. *Materials Science and Engineering A*, *430*(1–2), 189–202. https://doi.org/10.1016/j.msea.2006.05.125

Dempster, A. P., Laird, N. M., & Rubin, D. B. (1976). Maximum Likelihood from Incomplete Data via the EM Algorithm. *Royal Statistical Society*. Retrieved from https://dash.harvard.edu/handle/1/3426318

Elseifi, M. A., Al-Qadi, I. L., & Yoo, P. J. (2006). Viscoelastic modeling and field validation of flexible pavements. Journal of engineering mechanics, 132(2), 172-178. https://ascelibrary.org/doi/abs/10.1061/ 0733-9399

Fadil, H., Jelagin, D., & Larsson, P.-L. (2018). On the Measurement of two Independent Viscoelastic Functions with Instrumented Indentation Tests. *Experimental Mechanics*, *58*(2). https://doi.org/10.1007/s11340-017-0342-7

Fadil, H., Jelagin, D., Larsson, P.-L., & Partl, M. N. (2019). Measurement of the viscoelastic properties of asphalt mortar and its components with indentation tests. *Road Materials and Pavement Design*, *20*(sup2). https://doi.org/10.1080/14680629.2019.1628434

Fadil, H., Jelagin, D., & Partl, M. N. (2020). A new viscoelastic micromechanical model for bitumen-filler mastic. *Construction and Building Materials*, *253*, 119062. https://doi.org/10.1016/j.conbuildmat.2020.119062

Gudmarsson, A., Ryden, N., Di Benedetto, H., Sauzéat, C., Tapsoba, N., & Birgisson, B. (2014). Comparing Linear Viscoelastic Properties of Asphalt Concrete Measured by Laboratory Seismic and Tension–Compression Tests. *Journal of*

Nondestructive Evaluation, *33*(4), 571–582. https://doi.org/10.1007/s10921-014-0253-9

Hertz, H. (1881). Über die Berührung fester elastischer Körper. *Journal Für Die Reine Und Angewandte Mathematik*, *92*, 156–171. https://doi.org/10.1515/crll.1882.92.156

Jelagin, D., & Larsson, P. L. (2013). Measurement of the Viscoelastic Properties of Bitumen Using Instrumented Spherical Indentation. *Experimental Mechanics*, *53*(7), 1233–1244. https://doi.org/10.1007/s11340-013-9725-6

Johnson, K. L., & Keer, L. M. (1986). Contact Mechanics. In *Journal of Tribology* (Vol. 108). https://doi.org/10.1115/1.3261297

Lee, E. H., & Radok, J. R. M. (2011). The Contact Problem for Viscoelastic Bodies. *Journal of Applied Mechanics*, *27*(3), 438. https://doi.org/10.1115/1.3644020

Nynas AB. (2010). *Nynas 70/100 Paving Grade Bitumen Specifications*. Retrieved from https://notes.nynas.com/Apps/1112.nsf/wpds/GB_EN_Nynas_70_100/$File/Nynas_70_100_GB_EN_PDS.pdf

Ossa, E. A., & Collop, A. C. (2007). Spherical Indentation Behavior of Asphalt Mixtures. *Journal of Materials in Civil Engineering*, *19*(9), 753–761. https://doi.org/10.1061/(asce)0899-1561(2007)19:9(753)

Ossa, E. A., Deshpande, V. S., & Cebon, D. (2005). Spherical indentation behaviour of bitumen. *Acta Materialia*, *53*(11), 3103–3113. https://doi.org/10.1016/j.actamat.2005.01.040

Ulm, F. J., Vandamme, M., Bobko, C., Alberto Ortega, J., Tai, K., & Ortiz, C. (2007). Statistical indentation techniques for hydrated nanocomposites: Concrete, bone, and shale. *Journal of the American Ceramic Society*, *90*(9), 2677–2692. https://doi.org/10.1111/j.1551-2916.2007.02012.x

Zofka, A., & Nener-Plante, D. (2011). Determination of Asphalt Binder Creep Compliance Using Depth-Sensing Indentation. *Experimental Mechanics*, *51*(8), 1365–1377. https://doi.org/10.1007/s11340-011-9464-5